191 (2024) 206962

Contents lists available at ScienceDirect

Applied Catalysis O: Open

journal homepage: www.elsevier.com/locate/apcato

Unveiling the potential of alloyed core/double shell InZnP/ZnSe/ZnS quantum dots: High quantum efficiency and stable water splitting performance

Jeong-Mi Lee [a,b], Dong-Seog Kim [a], Bharagav Urupalli [a], Min-Sang Lee [c], Byung-Guk Ahn [a,*], Yeon-Tae Yu [a,*]

[a] Division of Advanced Materials Engineering, Research Center for Advanced Materials Development, Jeonbuk National University, Jeonju 54896, South Korea
[b] QDNT Co.,Ltd., Jeonju 54882, South Korea
[c] PLT Co.,Ltd., Gimje 54352, South Korea

ARTICLE INFO

Keywords:
Red quantum dots
Quantum yield
Cadmium-free
InZnP/ZnSe/ZnS
Core-shell

ABSTRACT

Economic and environment friendly synthesis of Cd-free core shell QDs has gained significant attention in the field of display devices and lighting applications. To amend the bottle neck of toxicity and to demonstrate the efficiency of metal chalcogenides-based systems, synthesis of high quantum efficiency QDs of InZnP/ZnSe/ZnS was targeted in the present work and achieved through two step optimization approach. To begin with, effect of temperature on core growth was optimized. Results delineate that high quantum efficiency was achieved at a precise core growth temperature of 190 °C. In addition to this, shell growth time preferential at 190 °C was derived in the second step, studies demonstrate that, a record quantum yield (PL QY) up to 95% was achieved with the 30-min shell growth time. Consecutive PEC studies evident the bifunctional HER and OER capabilities of as-prepared QDs. ST-3 shows an exceptional outcome of 8.25 mA/cm^2 (1 V vs RHE) as a photocathode, and 1.45 mA/cm^2 (2 V vs RHE) as a photo-anode. Detailed synthesis protocol and developed alloyed core/double-shell InZnP/ZnSe/ZnS red QDs with tunable emission across the visible spectrum give a notable insight for future studies in the fields of robust and sustainable optoelectronic applications.

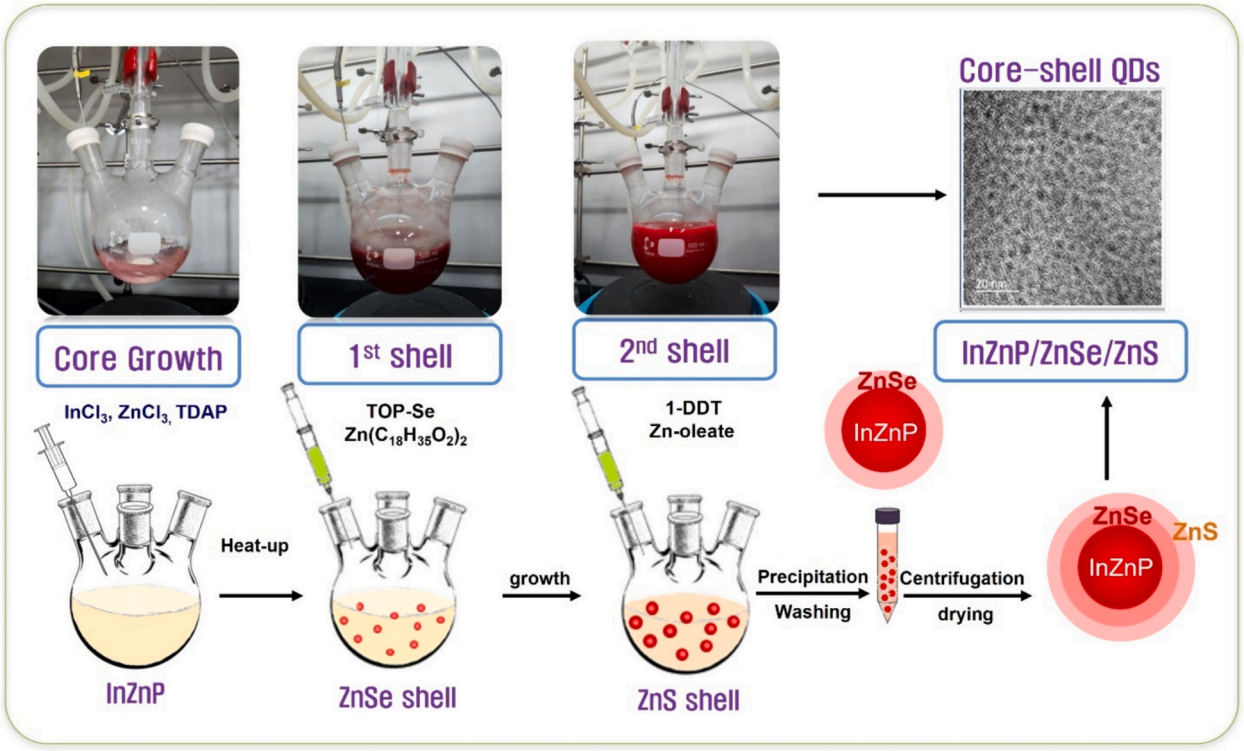
1. Introduction

Colloidal quantum dots (QDs) grab considerable interest in the current research trend due to their tunable and controllable optical properties and wide range of applications in light-emitting devices, photovoltaics, bio-imaging, and sensors [1]. Photocatalytic and photoelectrochemical (PEC) water splitting are two prominent avenues for the effective utilization of semiconductors including QDs for efficient water splitting [2]. In PEC the catalyst was deposited on a substrate and used as photo-anode or photo-cathode to strive the OER or HER successfully. In both the branches of water splitting, crucial factor to deal with is the preparation of an efficient catalytic component [3]. Hence, manifestation of efficient QDs could be highly feasible for sustainable energy production as well. Excellent PL QYs, along with finely tunable emission wavelengths, have enabled the successful commercial implementation of QDs as fluorescent materials in electric appliances. [4] To date, majority of high PL QY systems were reported in combination with Cd-based QDs, yet lack of chemical stability, toxicity of Cd based QDs, harm the society to an explicit extent. Accordingly, the development of non-cadmium based QDs with excellent quantum efficiency and stability becomes need of the hour. In line with this, the non-cadmium based QDs core materials such as the InP-based, ZnSe-based, CIS(CuInS)-based, and CZIS(CuZnInS)-based materials are being studied, and reported [5]. Among them, InP-based QDs were known to have excellent quantum efficiency, color purity and emission tunability ranging from visible to near-infrared region. [6] From the literary aspect [7], so far, the quantum efficiency of green QDs was reported to have over 95% on average, but red QDs efficiency remains only 80–90%. Thus, there is scope for the development of red QDs, to make such QDs with high stability.

Over the past two decades, the utilization of QDs in the field of photoelectrochemical (PEC) water splitting has seen a significant rise. However, a critical aspect remains under-addressed; the direct application of QDs as catalysts. The majority of reported studies utilize QDs as

* Corresponding authors.
E-mail addresses: bkahn@jbnu.ac.kr (B.-G. Ahn), yeontae@jbnu.ac.kr (Y.-T. Yu).

https://doi.org/10.1016/j.apcato.2024.206962
Received 27 March 2024; Received in revised form 25 May 2024; Accepted 27 May 2024
Available online 29 May 2024
2950-6484/© 2024 The Authors. Published by Elsevier B.V. This is an open access article under the CC BY-NC-ND license (http://creativecommons.org/licenses/by-nc-nd/4.0/).



Scheme. 1. Schmatic depiction of InZnP/ZnSe/ZnS QDs synthesis protocol.

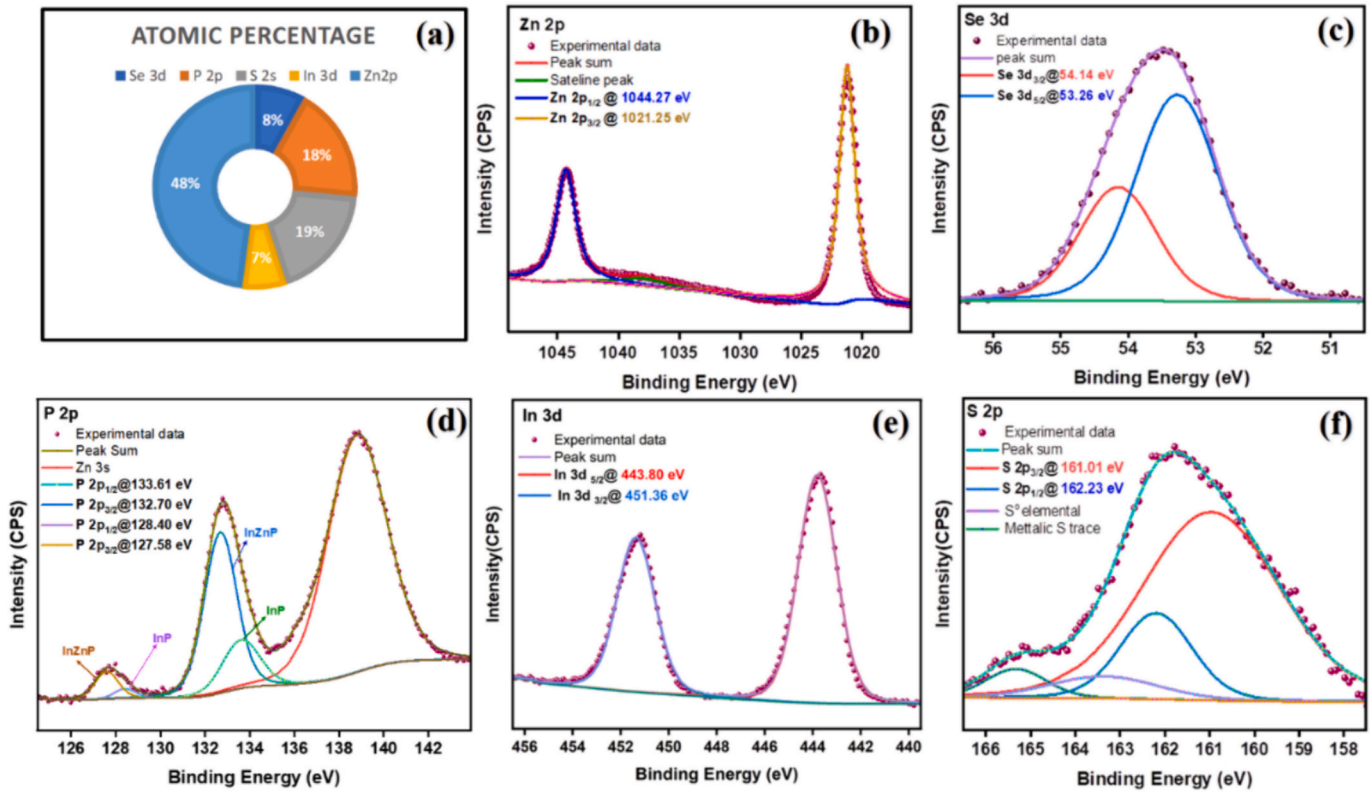


Fig. 1. (a) Atomic percentage of In, Zn, P, S and Se derived from XPS analysis, high resolution XPS of (b) Zn 2p (c) Se 3d (d) P 2p (e) In 3d t and (f) S 2p.

photosensitizers, decorating them onto semiconducting photo absorbers [8]. A wide range of well-studied semiconductors, including metal oxides (TiO_2, Fe_2O_3, ZnO, WO_3 etc) [9,10], metal sulfides (CdS, ZnS, Bi_2S_3, MoS_2) [11], g-C_3N_4 [12], and metal oxynitrides (TiO_xN_y, Fe_xO_yNz) [13], have been investigated with varying morphologies, phases, and heterojunction configurations for PEC water splitting and photocatalytic

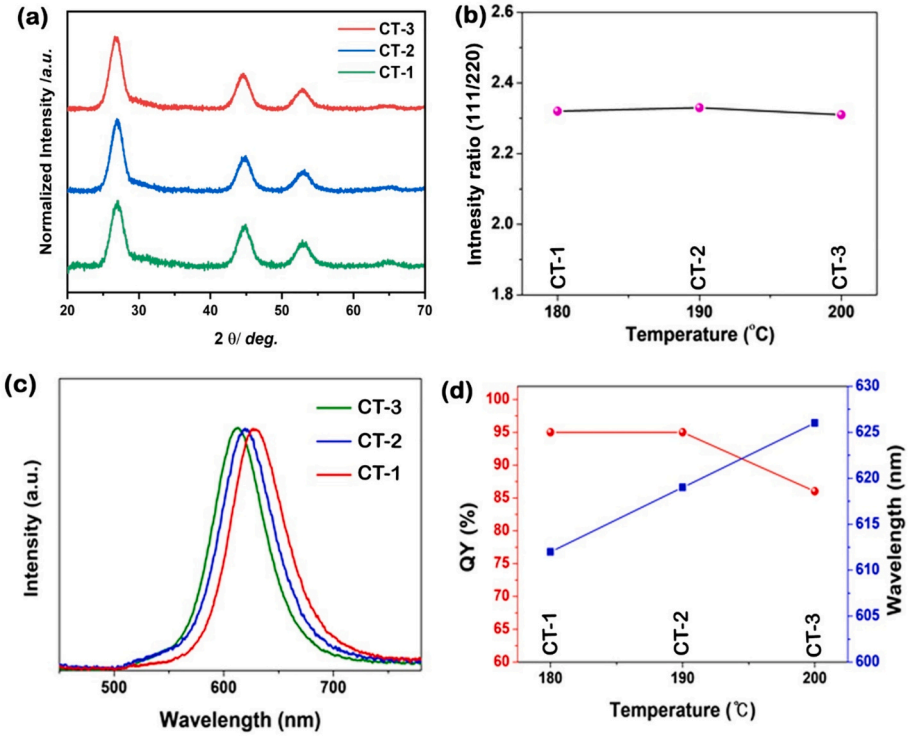


Fig. 2. (a) XRD patterns, (b) intensity ratio of (111)/ (220) of CT-1, CT-2, and CT-3. (c) PL spectra, (b) QY and PL peak position of CT-1, CT-2, and CT-3.

hydrogen evolution. Inspired by this landscape, we have chosen to explore the potential of high-quantum-yield QDs in PEC water splitting. Our approach goes beyond simply comparing photocurrent densities with previous reports. Instead, we present novel findings that explore a new pathway for utilizing QDs in this field.

Therefore, in this study, non-cadmium group III-II-V-based InZnP red QDs were synthesized by a solution process method. Further ZnSe gradient and ZnS shell were grown around the core with optimal core growth temperature and shell formation time. Upon optimization of afore said two, we have manifested the environmentally friendly (non-cadmium based) and highly efficient InZnP/ZnSe/ZnS alloyed core/double shell red QDs. This is an exclusive study that reveals the relationship between the crystallinity of InZnP alloy core and the QY of InZnP/ZnSe/ZnS QDs. Stable core generation and controlled shell growth manifested in the present work was successful in delivering the red QDs with 95% PLQY at the emission wavelength of 619 nm. PEC studies affirm the water splitting performance of the developed system with enhanced stability. Viable acquaintance of optimized InZnP/ZnSe/ZnS QDs as photo-anode and photo-cathode suggests the potential of utilizing the present system for futuristic electrocatalytic and photo-electrocatalytic systems. This study reports on the promising activity and stability of a first-time reported InZnP/ZnSe/ZnS photoelectrode for photoelectrochemical water splitting under solar irradiation.

2. Experimental section

2.1. Chemicals and reagents

Indium (III) chloride ($InCl_3$, 99.9% trace metals basis, Sigma Aldrich), Zinc chloride ($ZnCl_2$, reagent grade, ≥98%, Sigma Aldrich), Oleylamine (OLA, technical grade, 70%), Tris(diethylamine)phoshoine (DEAP, 97%, Sigma Aldrich), Zinc stearate ($ZnSt_3$, purum, 10–12% Zn basis, Sigma Aldrich),1-octadecene (ODE, technical grade, 90%, Sigma Aldrich), Tri-octyl phosphine (TOP, ≥98%, LAKE MATERIALS), Selenium (Se, pellets, <5 mm, ≥99.99% trace metals basis, Sigma Aldrich), Zinc acetate dehydrate ($Zn(OA)_2$, ACS reagent, ≥98%, Sigma Aldrich), Oleic acid (OA, technical grade, 90%, Sigma Aldrich), 1-dodecanethiol (1-DDT, ≥98%, Sigma Aldrich), n-hexane (96%, Samchun), Ethanol (99.9%, Samchun).

2.2. Synthesis protocol

2.2.1. Preparation of TOP-Se precursor

Selenium pellets 0.03 g were dissolved in 4 mL of TOP at RT inside a nitrogen glovebox.

2.2.2. Preparation of Zn-Oleate precursor

In a typical process, the $Zn(OA)_2$ (0.439 g) was mixed with 1.26 mL of oleic acid and 13.7 mL of ODE in around bottomed flask and subjected to heat treatment at 120 °C under vacuum for 2 h. Then, the flask was filled with N_2 and heated to 150 °C and kept for 1 h to form transparent clear solution. Finally, the mixture was cooled to room temperature (RT) and stored inside a glovebox in a scintillation vial.

2.2.3. Synthesis of InZnP/ZnSe/ZnS QDs

Herein, a representative synthesis method of InZnP/ZnSe/ZnS QDs is presented. 0.099 g of indium (III) chloride and 0.3 g of zinc chloride were mixed with 5 mL of OLA in a 50 mL three-neck flask and fixed to a Schlenk line with a reflux condenser. The mixture was heated to 120 °C under the vacuum for 2 h (vacuum level reaching 150 mTorr). Then, the flask was refilled with N_2 and the mixture was heated in the range of 180–200 °C and injected 0.35 mL of DEAP and maintained at that temperature for 30 min for the formation of InZnP core. TOP-Se and zinc stearate are then added to the above mixture three times at different temperatures to form the inner ZnSe shell. Herein the holding time was adjusted from 10 to 30 min during each addition of TOP-Se and zinc stearate. When the holding time is 10 min, the detailed description of this process is as follows. 1 mL of TOP-Se was injected to the flask and maintained at 220 °C for 10 min to form the inner ZnSe shell on the InZnP core. Next, 0.1 mmol of zinc stearate in 3 mL of ODE was injected to the flask and maintained at 240 °C for 10 min. Then, 1 mL of TOP-Se was injected to the flask and maintained at 260 °C for 10 min. Next, 0.1

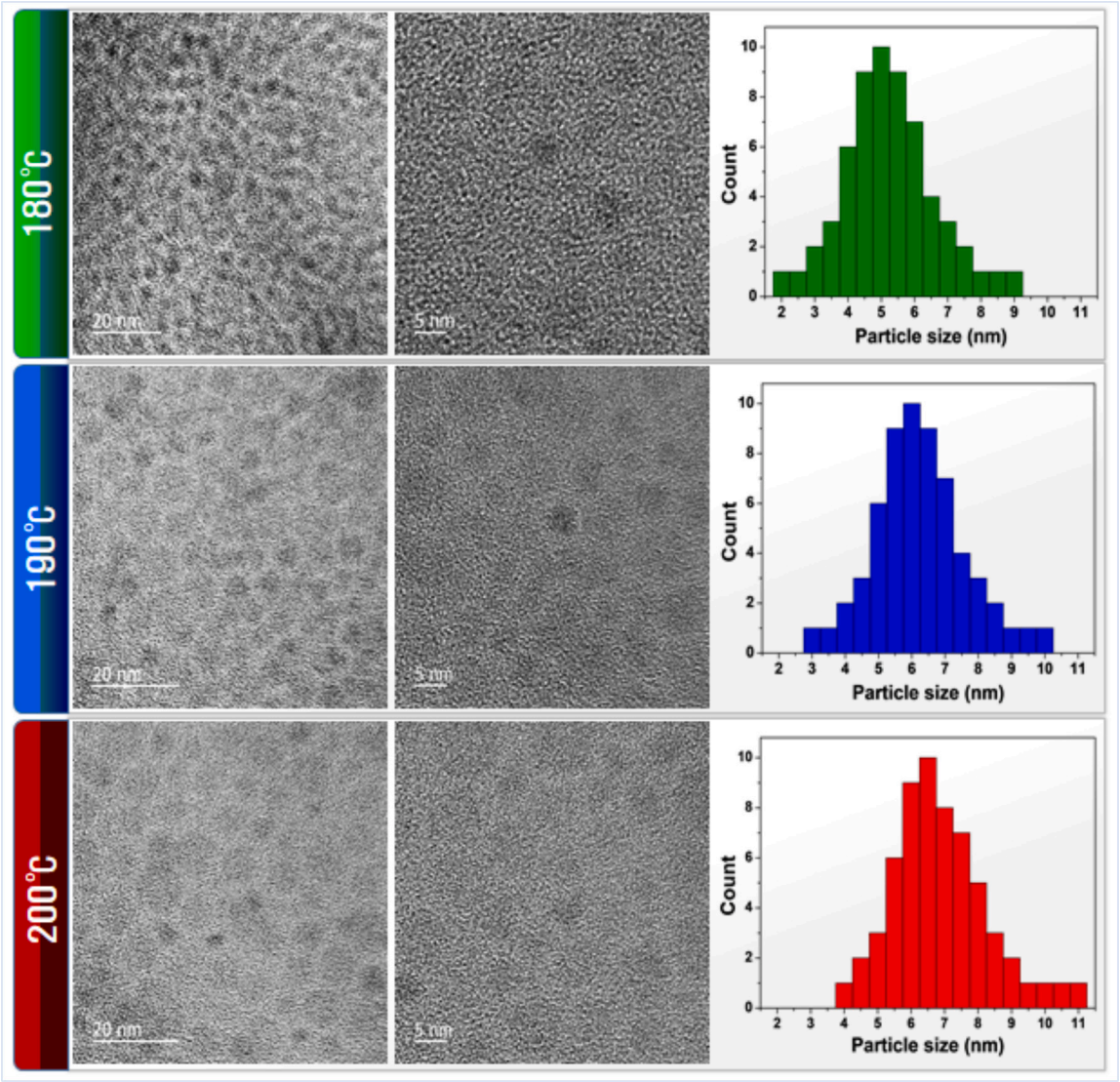


Fig. 3. TEM images, particle size distribution of InZnP/ZnSe/ZnS QDs synthesized with different core growth temperatures.

mmol of zinc stearate in 3 mL of ODE was injected to the flask and maintained at 280 °C for 10 min. Then, 1 mL of TOP-Se was injected to the flask and maintained at 300 °C for 10 min. Next, 0.1 mmol of zinc stearate in 3 mL of ODE was injected to the flask and maintained at 320 °C for 10 min. This mixture was cooled to 220 °C to form the outer ZnS shell, and 0.6 mL of 1-DDT was added and maintained at that temperature for 2 h. After that, the mixture was cooled to 190 °C, and 12 mL of Zn-oleate was added and maintained at that temperature for 1 h. A pictorial depiction of the detailed synthesis methodology can be seen in Scheme 1. After cooling to RT, the QDs were precipitated with 80 mL of ethanol and collected by centrifugation at 8000 rpm for 20 min. The synthesized QDs were dispersed in hexane, washed three times by adding ethanol to precipitate them, and finally stored in hexane and stored in a glove box filled with N_2.

3. Results and discussion

3.1. Chemical composition and valence state analysis

In depth chemical composition analysis was performed using monochromatic X-ray source of XPS and portrayed in Fig. 1. Along with valence state of Zn 2p, Se 3d, P 2p, In 3d and S 2p, atomic percentage was also attained, and presented in Fig. 1(a). Formation of alloyed core was evident from the Zn 2p (Fig. 1b), In 3d (Fig. 1e) metallic doublets and P 2p HR XP spectra depicted in Fig. 1 (d) [14,15]. Bonding between Zn and S evident from S $2p_{3/2}$ located at 161.01 eV as shown in Fig. 1(f). Metallic traces of S depict the excess and S richness in shell, which could be an indicative of alloyed core's subtle electronegativity [16]. Se $3d_{5/2}$ and Se $3d_{3/2}$ presence at respective binding energies of 53.26 eV and 53.14 eV affirms the Se bonding with Zn metallic species [17]. Zn 3 s found in P 2p spectra could be from Zn—S and oxidative layer formation between InZnP and ZnS Shell. Literature claims that this interface could serve as electron trap and strives the passive and uniform shell growth [18]. P 2p spectra shown in Fig. 1(d) exhibits high intensity $2p_{3/2}$ at 132.70 eV, and dwindled $2p_{3/2}$ at 127.58 eV, i.e., presence of single and bimetallic bindings of InP and InZnP axiomatically.

3.2. Effect of core-growth temperature: Structural and optical analysis

In the process of optimization of core growth with respect to temperature, InZnP core was grown individually for 25 min at 180 °C, 190 °C and 200 °C and labelled them as CT-1, CT-2, and CT-3 respectively. The X-ray diffraction patterns of CT-1, CT-2, and CT-3 were given in Fig. 2 (a). Peaks corresponds to (111), (220), and (311) are in good agreement with the InP phase. Fig. 2(b) depicts the derived intensity ratio between (111) and (220), to understand the deviation in

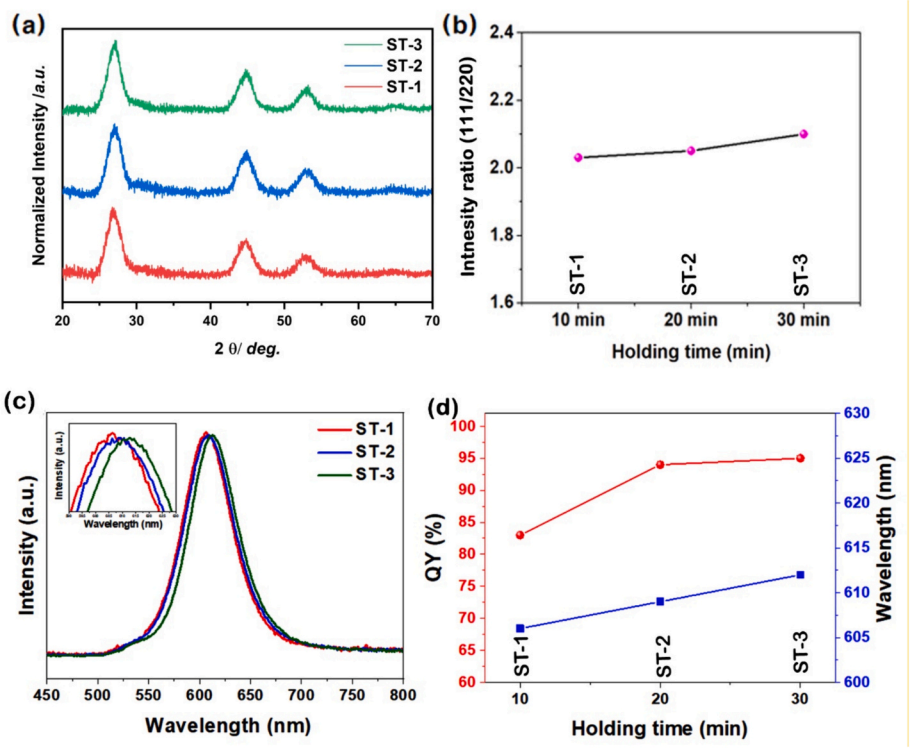


Fig. 4. (a) XRD patterns, (b) Intensity ratio of (111)/(220), (c) PL spectra, (d) QY and PL peak position of ST-1, ST-2, and ST-3.

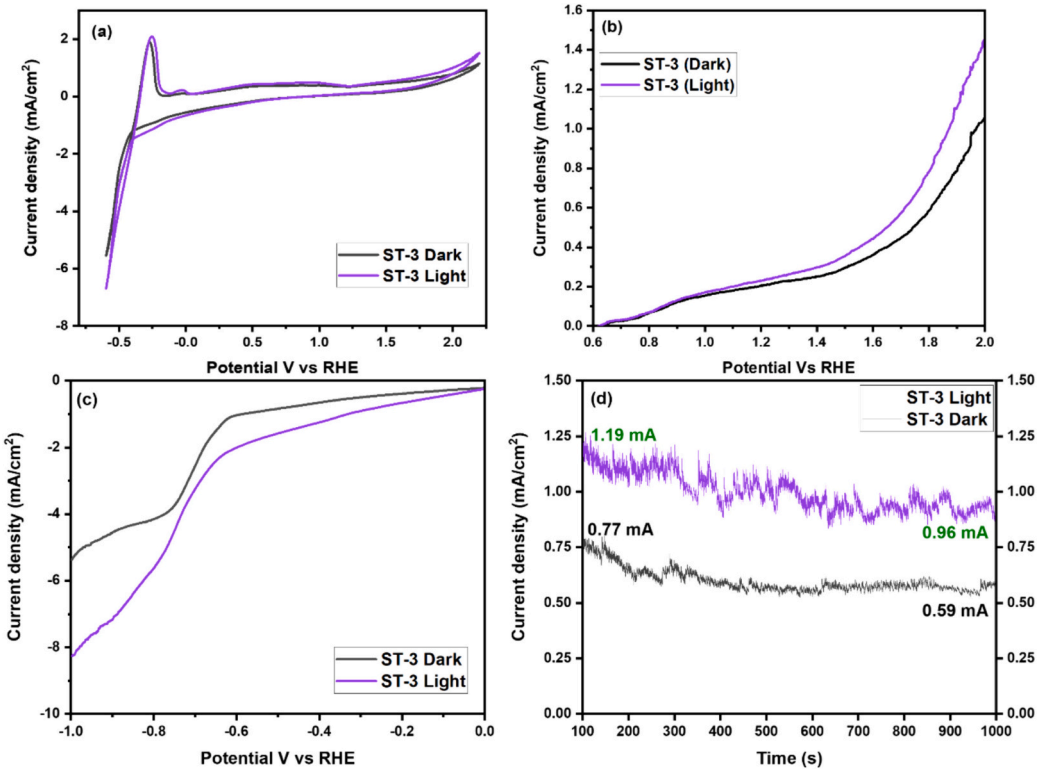


Fig. 5. (a) CV curves of ST-3, (b) J-V plots of ST-3 as photo-anode (OER), (c) J-V plots of ST-3 as photo-cathode (HER), (d) Chronoamperometry of ST-3 under dark and light illumination conditions.

crystallinity. In the temperature range from 180 to 200 °C, the crystallinity of the InZnP core was hardly changed. This was a good sign that the formation of core during this time frame was chemically stable and hence the crystallinity remained the same.

The PL efficiencies of CT-1, CT-2 and CT-3 were investigated further to evaluate the quantum yield and obtained results presented in Fig. 2 (c). CT-1, CT-2 and CT-3 shows the maximum peak intensity at 612 nm, 619 nm, and 626 nm respectively. QD has grown because of the Ostwald

ripening process, hence higher growth temperature of InZnP core can lead to large diameter of particles. The quantum yields of CT-1, CT-2 and CT-3 were evaluated and are presented along with the respective wavelengths in Fig. 2(d). QY evaluation evident that, CT-1 and CT-2 captures 95% quantum efficiency, whereas CT-3 shows dropped efficiency of 86%, this decreased efficiency could be due to the non-uniform shape of the particle.

3.3. Effect of core-growth temperature: morphological analysis

In line with the crystal structure analysis, morphological analysis was performed using TEM to understand the effect of core growth temperature on particle size of the QDs. CT-1, CT-2 and CT-3 were subjected to TEM analysis and obtained micrographs at different magnifications were depicted in Fig. 3 given below. From the micrographs and particle size analysis it was observed that the size of the QDs increased from 5 nm to 7 nm when the core growth temperature increased from 180 °C to 200 °C. Therefore, the quantum efficiency decreased. Hence the particle size order among the prepared three specimens is CT-1 > CT-2 > CT-3.

3.4. Effect of shell-growth time: structural and optical analysis

It is a known fact that the formation and growth of QDs are proportional to the time as well as temperature. In this study, when synthesizing a ZnSe shell to stably form InZnP/ZnSe/ZnS QDs, the holding times were changed to 10 min, 20 min, and 30 min respectively, at the same reaction temperature of 190 °C after injection of the Zn precursor and Se precursor. Fig. 4(a) shows the XRD patterns of ST-1, ST-2, and ST-3, the PL intensity and quantum efficiency of ST-2 was identical to the ST-3. Hence, the intensity ratio of prominent peaks corresponding to (111) and (220) planes were evaluated and compared, which can be seen in Fig. 4(b). When the holding time was set to 30 min, the intensity of crystallographic planes was highest. It indicates that the improved QY and the red shift can be due to the increment in crystallinity of InZnP/ZnSe/ZnS QDs (Fig. 4c). When the holding time for 10, and 30 min, the PL wavelength was 606 nm, and 612 nm, and quantum efficiency was 83%, and 95% respectively(Fig. 4d). As a result of maintaining it longer than that, there was no notable change.

3.5. Photoelectrochemical water splitting performance of ST-3

The electrocatalytic properties of ST-3 were systematically investigated within an alkaline and neutral aqueous environment. The methodology for fabricating the electrodes is comprehensively described in the supplementary information section S1. Cyclic voltammetry profiles, which elucidate the redox behavior of ST-3, are depicted in Fig. 5(a). An anodic pre-peak, discernible within the oxidation regime, is attributed to the adsorption of electroactive species onto the fluorine-doped tin oxide (FTO) substrate. A pronounced cathodic peak suggests a more favorable HER compared to the OER. Despite the apparent irreversibility of the CV curve, the electrocatalytic activity of ST-3, whether as a photo-anode or photo-cathode, is markedly high. The electrochemical performance of ST-3, with respect to HER, under both illumination and dark conditions, is presented in Fig. 5(b). At an applied potential of 1 V versus the reversible hydrogen electrode (RHE), the current densities achieved were 8.25 mA/cm^2 and 5.34 mA/cm^2 under light and dark conditions, respectively, as shown in Fig. 5(c). The bifunctional nature of the synthesized quantum dots is further evidenced by the OER current densities of 1.45 mA/cm^2 and 1.05 mA/cm^2 at 2 V versus RHE under light and dark conditions, respectively. These values are notably superior to those of many unmodified semiconductors such as ZnO which shows around 0.6 mA/cm^2 as photoanode [19,20].

For deep insight PEC analysis was checked in near neutral electrolyte medium as well with 1 M Na_2SO_4 (pH ≈ 7) instead of 1 M KOH, the results obtained were (Fig. S1) much lower than in the case of an alkaline medium. Cathodic currents were found to be 0.6 and 0.9 mA/cm^2 (1 V vs RHE) in dark and light conditions respectively. Water oxidation performance with ST-3 as photo-anode with 1 M Na_2SO_4 was also lower and found to be 0.54 and 0.68 mA/cm^2 (2 V vs RHE). Chronoamperometric studies were conducted on taking ST-3 as a photoanode using 1 M KOH and 1 M Na_2SO_4 at a constant voltage of 1.23 V vs RHE, the obtained CA on/off results were presented in Fig. S2. These results claim the potential of ST-3 as a robust photo electrocatalyst for both HER and OER in an alkaline medium, highlighting its bifunctional capabilities and the advantages of employing quantum dots in electrocatalysis. The stability of the electrocatalyst was examined at 1.8 V vs RHE to complement the activity, with stability. The results are presented in Fig. 5(d). After 1000 s of stability run at a constant potential, in both dark and light conditions, the depletion in photoelectrochemical water splitting performance was not >10%. After PEC analysis, the catalyst was collected and washed with distilled water for characterizing its crystallographic and optical absorbance properties. As obtained XRD and DRS-Uv results were depicted in Fig.S3 and S4 respectively. Post run characterizations further confirmed the stability of the prepared QD against the testing conditions. Hence the synthesized and optimized ST-3 was found to be a potential candidate and readily usable for diverse applications namely in display devices, Photocatalytic, photoelectrocatalytic, and electrocatalytic water splitting systems.

4. Conclusions

To improve the QY of core/shell InZnP/ZnSe/ZnS red QDs, the synthesis temperature of the InZnP alloy core and the formation time of ZnSe shell were optimized, and the effect of the crystallinity of the InZnP alloy core on the QY of InZnP/ZnSe/ZnS QDs was empirically investigated. The QY of InZnP/ZnSe/ZnS QD was optimized at the synthesis temperature of the InZnP alloy core of 190 °C, and even if the temperature was raised above that, the QY decreased due to the increase in the particle size of the QDs. On the other hand, increasing the reaction time for forming ZnSe, the middle shell of InZnP/ZnSe/ZnS QDs, to 30 min increased the crystallinity of the QDs, resulting in an increase in QY up to 95% at the emission wavelength of 619 nm. In support with the gleaned QY, the electrocatalytic water splitting performance of ST-3 was also examined under visible light spectrum and the results that emerged were found to be stable and efficient. The resulting efficiency was notable and can serve the upcoming studies for the development of highly efficient, non-toxic QDs in a robust and sustainable manner.

CRediT authorship contribution statement

Jeong-Mi Lee: Writing – original draft, Methodology, Conceptualization. **Dong-Seog Kim:** Validation, Methodology, Formal analysis, Data curation. **Bharagav Urupalli:** Writing – review & editing, Validation, Formal analysis, Data curation. **Min-Sang Lee:** Validation, Investigation, Data curation. **Byung-Guk Ahn:** Writing – review & editing, Validation, Formal analysis, Data curation, Conceptualization. **Yeon-Tae Yu:** Writing – review & editing, Supervision, Project administration, Investigation, Funding acquisition, Conceptualization.

Declaration of competing interest

The authors declare that they have no known competing financial interests or personal relationships that could have appeared to influence the work reported in this paper.

Data availability

Data will be made available on request.

Acknowledgments

This work was supported by 1) National Research Foundation of Korea (NRF) grant funded by the Korean government (MSIP) (2021R1A2C2008447), 2) project for "Academic-industrial-Research Collabo R&D" project (Grants No. S3301801(RS-2022-TI022957)) funded Korea Ministry of SMEs and Startups in 2022, and 3) the Industrial Technology Innovation Program funded by the Ministry of Trade, industry & Energy (MOTIE) [Grant No.10076464] of Korea.

Appendix A. Supplementary data

Supplementary data to this article can be found online at https://doi.org/10.1016/j.apcato.2024.206962.

References

[1] G. Xu, S. Zeng, B. Zhang, M.T. Swihart, K.-T. Yong, P.N. Prasad, New generation cadmium-free quantum dots for biophotonics and nanomedicine, Chem. Rev. 116 (2016) 12234–12327, https://doi.org/10.1021/acs.chemrev.6b00290.

[2] U. Bharagav, N.R. Reddy, V. Navakoteswara Rao, P. Ravi, M. Sathish, M. V. Shankar, T.M. Aminabhavi, R.R. Kakarla, M.M. Kumari, Z-scheme driven photocatalytic activity of CNTs-integrated Bi_2S_3/WO_3 nanohybrid catalysts for highly efficient hydrogen evolution under solar light irradiation, Chem. Eng. J. 465 (2023) 142886, https://doi.org/10.1016/j.cej.2023.142886.

[3] M.P. Ravikumar, T.A. Quach, B. Urupalli, K. Manjunatha, M.K. Murikinati, S. M. Venkatakrishnan, S.Y. Wu, T.O. Do, S. Mohan, Mechanistic insights into the phase formation of an atypical iron oxynitride (FexOyNz) system and its multifunctional photocatalytic applications, ACS Sustain. Chem. Eng. 11 (2023) 17272–17284, https://doi.org/10.1021/acssuschemeng.3c04497.

[4] E. Jang, H. Jang, H.A. Kang, O. Cho, 67-1: invited paper: environmentally friendly quantum dots for display applications, SID Symp. Dig. Tech. Pap. 48 (2017) 980–983, https://doi.org/10.1002/sdtp.11824.

[5] Z. Bai, W. Ji, D. Han, L. Chen, B. Chen, H. Shen, B. Zou, H. Zhong, Hydroxyl-terminated CuInS2 based quantum dots: toward efficient and bright light emitting diodes, Chem. Mater. 28 (2016) 1085–1091, https://doi.org/10.1021/acs.chemmater.5b04480.

[6] P. Ramasamy, N. Kim, Y.-S. Kang, O. Ramirez, J.-S. Lee, Tunable, bright, and narrow-band luminescence from colloidal indium phosphide quantum dots, Chem. Mater. 29 (2017) 6893–6899, https://doi.org/10.1021/acs.chemmater.7b02204.

[7] F. Pietra, L. De Trizio, A.W. Hoekstra, N. Renaud, M. Prato, F.C. Grozema, P. J. Baesjou, R. Koole, L. Manna, A.J. Houtepen, Tuning the lattice parameter of InxZnyP for highly luminescent lattice-matched core/shell quantum dots, ACS Nano 10 (2016) 4754–4762, https://doi.org/10.1021/acsnano.6b01266.

[8] A. Ikram, M. Zulfequar, V.R. Satsangi, Role and prospects of green quantum dots in photoelectrochemical hydrogen generation: a review, Int. J. Hydrog. Energy 47 (2022) 11472–11491, https://doi.org/10.1016/j.ijhydene.2022.01.187.

[9] N. Ramesh Reddy, U. Bhargav, M. Mamatha Kumari, K.K. Cheralathan, M. Sakar, Review on the interface engineering in the carbonaceous titania for the improved photocatalytic hydrogen production, Int. J. Hydrog. Energy 45 (2020) 7584–7615, https://doi.org/10.1016/j.ijhydene.2019.09.041.

[10] S. Chandrappa, D.H.K. Murthy, N.L. Reddy, S.J. Babu, D. Rangappa, U. Bhargav, V. Preethi, M. Mamatha Kumari, M.V. Shankar, Utilizing 2D materials to enhance H_2 generation efficiency via photocatalytic reforming industrial and solid waste, Environ. Res. 200 (2021) 111239, https://doi.org/10.1016/j.envres.2021.111239.

[11] U. Bharagav, N.R. Reddy, V.N. Koteswararao, P. Ravi, P. K, M. Sathish, K. K. Cheralathan, M.V. Shankar, M.M. Kumari, Heterojunction of CdS Nanocapsules-WO3Nanosheets composite as a stable and efficient photocatalyst for hydrogen evolution, Energy Fuel 34 (2020) 14598–14610, https://doi.org/10.1021/acs.energyfuels.0c00597.

[12] U. Bharagav, N. Ramesh Reddy, V. Nava Koteswara Rao, P. Ravi, M. Sathish, D. Rangappa, K. Prathap, C. Shilpa Chakra, M.V. Shankar, L. Appels, T. M. Aminabhavi, R.R. Kakarla, M. Mamatha Kumari, Bifunctional g-C_3N_4/carbon nanotubes/WO_3 ternary nanohybrids for photocatalytic energy and environmental applications, Chemosphere 311 (2023) 137030, https://doi.org/10.1016/j.chemosphere.2022.137030.

[13] M.P. Ravikumar, T.A. Quach, B. Urupalli, S. Kumar, Y.P. Fu, M.K. Murikinati, S. Muthukonda Venkatakrishnan, T.O. Do, S. Mohan, Phase engineering of titanium oxynitride system and its solar light-driven photocatalytic dye degradation, H2 generation, and N2 fixation properties, ACS sustain, Chem. Eng. 11 (2023) 15192–15206, https://doi.org/10.1021/acssuschemeng.3c02715.

[14] M. Burkitt-Gray, M. Casavola, P.C.J. Clark, S.M. Fairclough, W.R. Flavell, R. A. Fleck, S.J. Haigh, J.C.R. Ke, M. Leontiadou, E.A. Lewis, J. Osiecki, B. Qazi-Chaudhry, G. Vizcay-Barrena, W. Wichiansee, M. Green, Structural investigations into colour-tuneable fluorescent InZnP-based quantum dots from zinc carboxylate and aminophosphine precursors, Nanoscale 15 (2022) 1763–1774, https://doi.org/10.1039/d2nr02803d.

[15] J.H. Jo, D.Y. Jo, S.H. Lee, S.Y. Yoon, H.B. Lim, B.J. Lee, Y.R. Do, H. Yang, InP-based quantum dots having an InP core, composition-gradient ZnSeS inner Shell, and ZnS outer shell with sharp, bright emissivity, and blue absorptivity for display devices, ACS Appl. Nano Mater. 3 (2020) 1972–1980, https://doi.org/10.1021/acsanm.0c00008.

[16] E.M. Jubeer, M.A. Manthrammel, P.A. Subha, M. Shkir, K.P. Biju, S.A. AlFaify, Defect engineering for enhanced optical and photocatalytic properties of ZnS nanoparticles synthesized by hydrothermal method, Sci. Rep. 13 (2023) 16820, https://doi.org/10.1038/s41598-023-43735-1.

[17] J.R. Shallenberger, N. Hellgren, Zinc selenide analyzed by XPS, Surf. Sci. Spectra. 27 (2020), https://doi.org/10.1116/6.0000165.

[18] D.A. Granada-Ramirez, J.S. Arias-Cerón, M.L. Gómez-Herrera, J.P. Luna-Arias, M. Pérez-González, S.A. Tomás, P. Rodríguez-Fragoso, J.G. Mendoza-Alvarez, Effect of the indium myristate precursor concentration on the structural, optical, chemical surface, and electronic properties of InP quantum dots passivated with ZnS, J. Mater. Sci. Mater. Electron. 30 (2019) 4885–4894, https://doi.org/10.1007/s10854-019-00783-6.

[19] X. Long, T. Wang, J. Jin, X. Zhao, J. Ma, The enhanced water splitting activity of a ZnO-based photoanode by modification with self-doped lanthanum ferrite, Nanoscale 13 (2021) 11215–11222, https://doi.org/10.1039/d1nr02673a.

[20] N.R. Reddy, P.M. Reddy, N. Jyothi, A.S. Kumar, J.H. Jung, S.W. Joo, Versatile TiO_2 bandgap modification with metal, non-metal, noble metal, carbon material, and semiconductor for the photoelectrochemical water splitting and photocatalytic dye degradation performance, J. Alloys Compd. 935 (2023) 167713, https://doi.org/10.1016/j.jallcom.2022.167713.